Editors' Suggestion

Blue Phosphorene Bilayer Is a Two-Dimensional Metal and an Unambiguous Classification Scheme for Buckled Hexagonal Bilayers

Jessica Arcudia,[1] Roman Kempt,[2] Miguel Eduardo Cifuentes-Quintal,[1] Thomas Heine,[2,3,4,*] and Gabriel Merino[1,†]

[1]*Departamento de Física Aplicada, Centro de Investigación y de Estudios Avanzados, Unidad Mérida, 97310, Mérida, Yucatán, México*

[2]*Technische Universität Dresden, Fakultät für Chemie und Lebensmittelchemie, Bergstraße 66c, 01062 Dresden, Germany*

[3]*Helmholtz Zentrum Dresden-Rossendorf, Leipzig Research Branch, Permoserstr. 15, 04318 Leipzig, Germany*

[4]*Department of Chemistry, Yonsei University, Seodaemun-gu, Seoul 120-749, Republic of Korea*

(Received 21 July 2020; accepted 10 September 2020; published 3 November 2020)

High-level first-principles computations predict blue phosphorene bilayer to be a two-dimensional metal. This structure has not been considered before and was identified by employing a block-diagram scheme that yields the complete set of five high-symmetry stacking configurations of buckled honeycomb layers, and allows their unambiguous classification. We show that all of these stacking configurations are stable or at least metastable both for blue phosphorene and gray arsenene bilayers. For blue phosphorene, the most stable stacking arrangement has not yet been reported, and surprisingly it is metallic, while the others are indirect band gap semiconductors. As it is impossible to interchange the stacking configurations by translations, all of them should be experimentally accessible via the transfer of monolayers. The metallic character of blue phosphorene bilayer is caused by its short interlayer distance of 3.01 Å and offers the exceptional possibility to design single elemental all-phosphorus transistors.

DOI: 10.1103/PhysRevLett.125.196401

Introduction.—Since the first exfoliation of graphene and the discovery of its remarkable properties [1], many other 2D materials came in the focus of interest, including its isoelectronic hexagonal congener boron nitride [2], and the wide variety of transition metal dichalcogenides [3–5]. However, it was not before the exfoliation black phosphorus [6,7] that the attention for 2D pnictogens emerged. Black phosphorus is the most stable allotrope of phosphorus and crystallizes in an orthorhombic structure. But a single layer of phosphorus, so-called phosphorene, can also crystallize in other forms. The honeycomb structure predicted by Zhu and Tománek [8] is just 2 meV/atom higher in energy than the black counterpart, and given that its band gap value is slightly above the photon energy of visible blue light, it was named blue phosphorene (in the following blue P). This prediction was materialized just a couple of years later by Zhang *et al.*, who successfully synthesized monolayer (ML) blue P by epitaxial growth on an Au(111) substrate [9]. The next pnictogen of interest is arsenic, mostly found in its bulk form as gray arsenic, and whose layered rhombohedral structure makes it an excellent candidate for exfoliation. The first studies on the stability and the properties of a single arsenic layer, i.e., gray arsenene (in the following gray As), predicted by Kamal and Ezawa [10] and Kou *et al.* [11], encouraged experimental groups to exfoliate few-layers arsenic [12].

Both blue P and its arsenic congener gray As have a structure similar to graphene, which is a hexagonal lattice with their atoms alternatingly being displaced out of the 2D plane [Fig. 1(a)]. These monolayers show exciting electronic properties with an indirect band gap in the range of 1.5–2.0 eV [8–10,12]. blue P is a *p*-type semiconductor

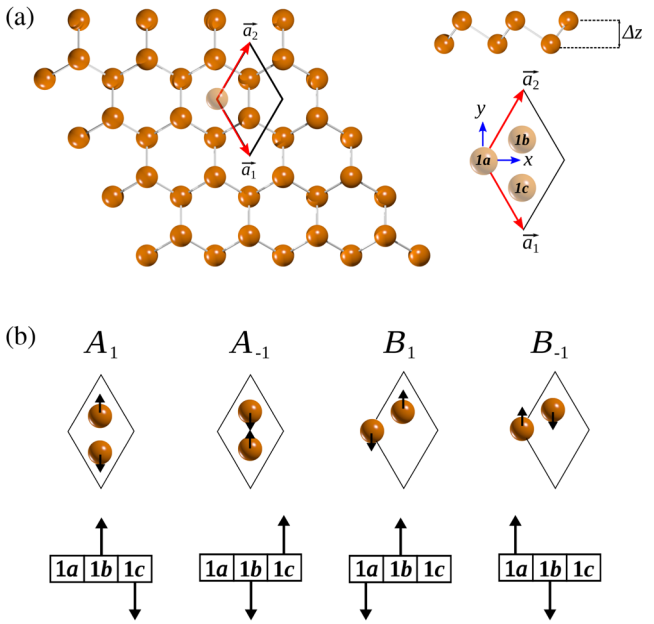

FIG. 1. (a) Front and side view of a buckled honeycomb monolayer. The unit cell with its lattice vectors and high symmetry sites 1*a*, 1*b*, and 1*c*. (b) Top: four different representations of a unit cell (arrows indicate the out of plane displacement of the atoms); bottom: block diagrams represent each monolayer.

with high carrier mobility [13]. On the other hand, gray As could be used for transistors or mechanical sensors, due to its indirect-direct band gap transitions [11,14], semiconductor-metal transitions [8,10], and topological phase transitions under strain [15,16].

It is well known that interlayer interactions can significantly alter the properties of 2D materials, most strikingly discussed recently for superconductivity in bilayer (BL) graphene [17,18] but also for band gap nature and valleytronics in transition-metal dichalcogenides (for a review, see Ref. [19]) or for metal-insulator transitions in noble metal chalcogenides (for a review, see Ref. [20]). The properties crucially depend on the stacking type and twist angle, which can be controlled using various transfer techniques [21].

Only a few studies addressed interlayer effects in blue P and gray As, and no details on the stacking order have been reported experimentally up to now [9,12]. Given the corrugation of the monolayer, more than the high-symmetry *AA* and *AB* stacking orders are expected. In how many ways is it possible to stack them? Even for the simplest case of two buckled honeycomb layers, this question has not been answered yet. Herein, we suggest a new approach based on a simple graphical analysis, which we will call a "block diagram" to ascertain it.

Using block diagrams, we identify all possible high-symmetry stacking configurations of BL buckled honeycomb lattices, which are expected to yield all low-energy forms for blue P and gray As bilayers.

Employing first principles calculations [density-functional theory (DFT), the random phase approximation (RPA), and single-particle Green's function approach G_0W_0], we calculated their structures and thermodynamic stabilities, and explore their electronic structures. We discovered that the lowest-energy blue P BL was not yet reported to date and, surprisingly, it is metallic.

Results and discussion.—Because both blue P and gray As crystallize in the trigonal lattice, we can describe a single layer in the subperiodic layer group **P**3 (#65) with the unique sites $1a = (0, 0, z)$, $1b = (1/3, 2/3, z_1)$, and $1c = (2/3, 1/3, z_2)$, where two sites are occupied with $z_1 = -z_2$ [22].

The lattice vectors ($\vec{a}_1$ and $\vec{a}_2$) delimiting the two-dimensional lattice are defined as $\vec{a}_1 = \frac{1}{2}a\hat{x} - (\sqrt{3}/2)a\hat{y}$, $\vec{a}_2 = \frac{1}{2}a\hat{x} + (\sqrt{3}/2)a\hat{y}$, where a is the lattice constant. Then the unit cells of any trigonal monolayer with a buckling can be represented as in Fig. 1(b), where the arrows indicate the out-of-plane displacements. We conveniently label these forms as A_1, A_{-1}, B_1, and B_{-1}, where the negative sign in the subscripts denotes a displacement change of the atoms with respect to the plane (up or down). These four configurations are symmetry equivalent and can be used for the construction of the BL forms. For a better understanding, we design a simple graphical method, which we call "block diagram" to facilitate the visualization.

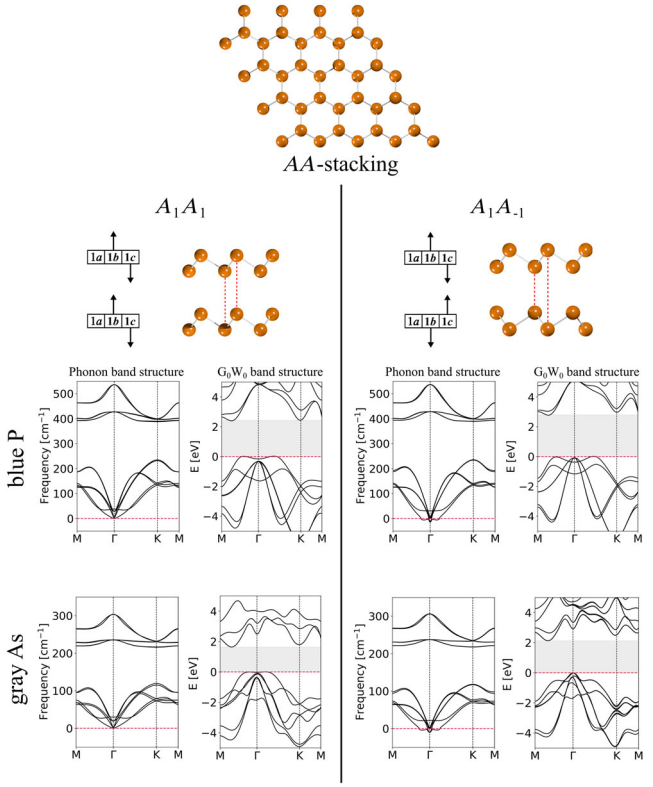

FIG. 2. Top view of an *AA*-type bilayer. The block diagram, atomistic structure, and phonon and electronic band structures of its two configurations: A_1A_1, and A_1A_{-1}.

This block diagram is divided into three parts, and each of them specifies a site of the unit cell ($1a$, $1b$, or $1c$). The atoms occupy two of the three sites and the direction of the arrows is related to the buckling. So, to build a bilayer, one puts another block on the top. In this way, we identify the total number of different high-symmetry forms of corrugated honeycomb bilayer as five, where the stacking sequence of two of them is of *AA* type, and for the remaining three it is *AB* type (see block diagrams in Figs. 2 and 3). These five stacking configurations are reported for silicene, whose layers are covalently bound [23].

For BL blue P, only four different stacking configurations have been studied to date [24,25]. First principles calculations indicated the A_1A_1 configuration to be the most stable one, followed by $A_1B_1, A_{-1}B_1$, and A_1A_{-1}. For gray As, there is an on-going debate whether the A_1B_{-1} or the A_1A_1 form is the most stable one [25–28].

For all stable and metastable stacking configurations discussed in this work, full geometry optimizations yield similar structural parameters, independent on the density-functional, the choice of London dispersion correction scheme, the orbital representation (local basis functions vs plane waves), or the underlying code (see the methods section for details). In all but one case a single local minimum per stacking configuration is found. Only for the

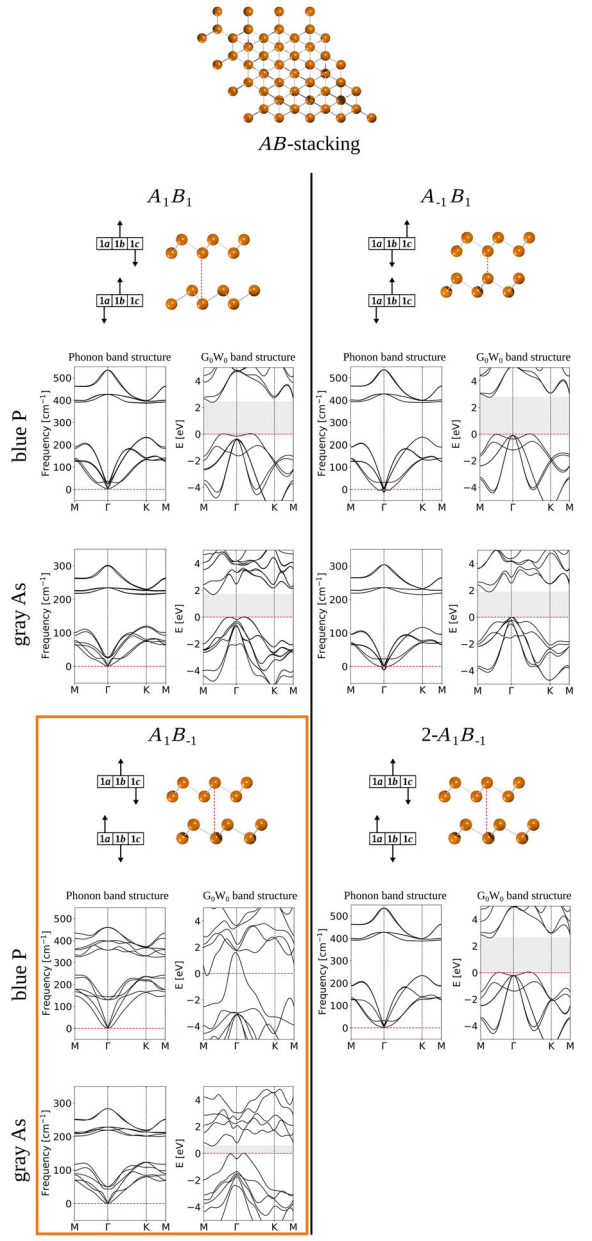

FIG. 3. Top view of an AB-type bilayer. The block diagram, atomistic structure, and phonon and electronic band structures of its three configurations: A_1B_1, $A_{-1}B_1$, and A_1B_{-1}. The second minimum of A_1B_{-1} $(2-A_1B_{-1})$ is included. The most stable stacking configuration is indicated by a frame.

A_1B_{-1} configuration of blue P we found two local minima: one minimum corresponds to a structure where the interlayer distance d is small (3.01 Å) and shows small corrugation, corresponding to a smaller buckling height Δz. We call this structure A_1B_{-1}. The second structure $(2-A_1B_{-1})$ shows a larger interlayer distance of 4.93 Å, corresponding to weakly interacting layers, and larger buckling. Both for blue P and gray As BL the closer interlayer distance in A_1B_{-1} is accompanied by a lattice constant increase of 0.1 Å and by a buckling reduction of

TABLE I. The lattice constant (a), buckling height (Δz), and interlayer distance (d), computed at the PBE + MBD level for blue P and gray As bilayers.

	blue P BL			gray As BL		
System	a (Å)	Δz (Å)	d (Å)	a (Å)	Δz (Å)	d (Å)
A_1B_{-1}	3.36	1.17	3.01	3.69	1.35	3.66
A_1A_1	3.26	1.24	4.66	3.60	1.40	4.58
A_1B_1	3.27	1.24	4.68	3.61	1.40	4.38
$2-A_1B_{-1}$	3.27	1.24	4.93	⋯	⋯	⋯
$A_{-1}B_1$	3.26	1.24	5.36	3.59	1.40	5.43
A_1A_{-1}	3.26	1.24	5.42	3.59	1.40	5.48
Monolayer	3.26	1.24	⋯	3.60	1.40	⋯

$\Delta z \approx 0.07$ Å. The remainder of the structures has almost identical lattice constants and buckling heights as the monolayer ($a = 3.26$ Å and $\Delta z = 1.24$ Å, Table I) [9,29]. Structural parameters for all stacking configurations of BL blue P and gray As are summarized in Table I.

All investigated BL systems are significantly more stable than their ML counterparts and are unlikely to exfoliate without severe intrusion. For both blue P and gray As, the A_1B_{-1} stacking configuration was found to be the most stable one. In both cases, this structure has distinct features making it quite different compared to the other configurations: It has the smallest interlayer distance and the smallest corrugation. The interlayer binding energy, defined as $E_{ib} = (E_{\mathrm{BL}} - 2E_{\mathrm{ML}})/N$, exceeds 180 meV per atom in both cases (Table II). It is important to note that local and hybrid density functionals give different stacking orders for the stacking configurations, which result in disagreement on the most stable form. Substantiation at the RPA level, independent if starting from a Perdew, Burke, and Ernzerhof (PBE) or PBE0 calculation, result in the same stacking order and clearly identify A_1B_{-1} to be the most stable form.

For blue P A_1B_{-1} BL, we show an abrupt change in buckling height Δz and the distance between layers d upon

TABLE II. The relative energies (ΔE) and the interlayer binding energy (E_{ib}) for all hexagonal blue phosphorene and gray arsenene stacking configurations, computed at the RPA + RSE@PBE0 level (including the ZPE correction). Units are in meV/atom.

	blue P BL		gray As BL	
System	ΔE	E_{ib}	ΔE	E_{ib}
A_1B_{-1}	0.0	−180.2	0.0	−185.2
A_1A_1	83.9	−96.2	25.7	−159.5
A_1B_1	86.8	−93.4	16.1	−169.0
$2-A_1B_{-1}$	104.1	−76.1	⋯	⋯
$A_{-1}B_1$	126.2	−54.0	108.9	−76.3
A_1A_{-1}	128.4	−51.8	96.5	−88.6

variation of lattice constant a, corresponding to the phase transition from the metallic configuration A_1B_{-1} to the semiconducting configuration $2-A_1B_{-1}$ [see Figs. S1(a) and S1(b) in the Supplemental Material [30]). In Fig. S1(c) we plot the buckling height Δz vs the energy difference ΔE, indicating that A_1B_{-1} is energetically favorable as it is less corrugated. Figure S1(d) indicates that A_1B_{-1} is extremely sensitive to variations in the interlayer distance d. $2-A_1B_{-1}$ shows weaker interlayer interactions and is located in the second, very shallow minimum.

While for BL blue P the configuration A_1B_{-1} is by far the most stable one, for BL gray As two configurations are energetically competitive: A_1A_1 and A_1B_1 are only less than 26 meV per atom higher in energy. Relative energies with respect to the monolayers and with respect to the most stable bilayer forms are given in Table II.

The phonon dispersion of the blue P and gray As MLs show the typical features of 2D materials, with two linear and one out-of-plane quadratic branches of the acoustic modes, and a clear energetic separation of optical and acoustic branches (Fig. S2). For blue P and gray As BL systems (Figs. 2 and 3), the phonon dispersion significantly differs between the most stable A_1B_{-1} and the other structures: while for all systems the three acoustic modes are in the same energy range as three low-energy optical modes (emerging from the second bilayer system and indicating weaker interactions), for A_1B_{-1} the stronger interlayer interaction lifts the low-energy optical modes towards higher energies and these branches show significantly less dispersion compared to the other stacking configurations. These shifted vibrational modes are of E_g and A_g symmetry and Raman active, and thus could serve for the characterization of this BL, similar as it has been demonstrated for graphene and silicene experimentally [31]. For the high-energy arrangements $A_{-1}B_1$ and A_1A_{-1} of both blue P and gray As BLs we found small imaginary frequencies which are due to the limitations of the numerical approach used in the phonon calculations.

To substantiate the electronic band gaps, the electronic structures have been recalculated within the quasiparticle approach, using the single-shot G_0W_0 approximation on top of PBE Kohn-Sham bands. Spin-orbit coupling (SOC) was included in all calculations for the gray As systems (see Table III). Besides the well-known band gap underestimation, the limitations of local DFT calculations also include the incorrect location of the valence band maximum for blue P (see also Fig. S3) [32].

Most importantly, both DFT and G_0W_0 identify blue P BL in the most stable configuration A_1B_{-1} as a metal. All other systems are indirect band gap semiconductors, with the G_0W_0 band gaps being considerably larger compared to those calculated by PBE. For BL blue P, electronic band gaps range from 2.39 to 2.82 eV, values that are lower than those of the ML (3.25 eV). For gray As, the A_1B_{-1} low-energy form has a remarkably small band gap of 0.58 eV, while the other systems range from 1.38 to 2.04 eV, thus being somewhat narrower than that of the ML (2.30 eV). For all semiconducting blue P and gray As BLs we found an interesting competition of a parabolic band climaxing at the Γ point and a Mexican hat structure around Γ point to become the valence band maximum. The latter is obtained for blue P BL in A_1A_1 and A_1B_1 configuration (somewhat less pronounced for gray As BL). A similar Mexican hat structure has been reported for GaSe and other III-VI monolayers, and the small dispersion may be useful for small FET structures and could give rise to Landau levels [33,34].

TABLE III. Indirect band gaps (E_{gap}) of ML and BL stacking configurations of blue P and gray As calculated at PBE and G_0W_0 levels of theory. Units are in eV. SOC was considered for the gray As systems.

	E_{gap}-blue P		E_{gap}-gray As	
System	PBE	G_0W_0	PBE-SOC	G_0W_0-SOC
A_1B_{-1}	...	...	0.12	0.58
A_1A_1	1.23	2.39	0.84	1.64
A_1B_1	1.25	2.40	0.63	1.38
$2-A_1B_{-1}$	1.41	2.59	...	...
$A_{-1}B_1$	1.58	2.80	1.27	2.04
A_1A_{-1}	1.60	2.82	1.22	1.99
Monolayer	1.96	3.25	1.43	2.30

Finally, we return to the remarkable 2D metal A_1B_{-1} blue P. The band structure (Fig. 3) includes metallic bands crossing the Fermi level near the Γ point, characterizing it as conventional metal. In addition, there is a basin of charge carriers close to M point. This interesting band structure suggests anisotropic electronic properties that shall not be further explored at this stage.

Summary and outlook.—We present a scheme to identify and to label all symmetrically distinct stacking configurations of corrugated honeycomb bilayers and investigate the resulting structures blue P and gray As. We discovered a new, and a the same time the most stable, configuration of blue P, which has a small interlayer distance, quenched corrugation and is a new member of the exclusive group of two-dimensional metals.

Besides the most stable A_1B_{-1} form, also A_1A_1 and A_1B_1 stacking configurations could be obtained experimentally by layer transfer techniques, as their large interlayer interaction and symmetry constraints prevent interconversion or relaxation into other structures. Lower-symmetry configurations as they are known for BL graphene are unlikely here due to the surface corrugation. This holds both for blue P and gray As. Except for the metallic blue P A_1B_{-1} form, all investigated blue P and gray As bilayers are indirect band gap semiconductors and resemble the Mexican hat-type feature of the electronic bands near the valence band maximum which have been intensively discussed for III-VI-group mono- and multilayer systems.

Blue P shows a semiconductor-metal transition when going from the ML to the most stable BL. Such transitions have been found for other 2D materials (e.g., noble metal chalcogenides [35] and GeP_3 [36]) and could be used to design single-material transistors with low Schottky barrier between the electrode and semiconducting scattering region [37]. In a similar vein, we think it is a remarkable challenge to construct the first single-element transistor based on blue phosphorus, with its metallic bilayer configuration serving as electrode material.

Methods.—To identify all potentially existing isomeric structures, we started geometry optimization with different starting structures, varying interlayer distances and buckling. All geometries have been fully optimized by means of DFT within the framework of the projector-augmented wave method [38,39] as implemented in the Vienna *ab initio* simulation package (VASP 5.4.4) [40,41].

The valence states were expanded in plane waves with an energy cutoff of 400 eV. The PBE exchange-correlation functional was employed [42], with London dispersion interactions taken into account by the many-body dispersion (MBD) correction as suggested by Tkatchenko and coworkers [43]. For comparison, we also used the Barone and Adamo's hybrid PBE0 functional [44,45] which does not affect the geometries of the bilayers. The first Brillouin zone was sampled using a Γ-centered k grid of $15 \times 15 \times 1$ and $42 \times 42 \times 1$ k points for hexagonal phosphorene and arsenene bilayers, respectively, and Gaussian smearing of 0.10 eV. These numerical parameters were chosen to ensure a convergence criterion of 10^{-8} eV in total energy, and 10^{-3} eV/Å in atomic forces. A vacuum space of 25 Å was considered in order to avoid interactions with the repeated images. The lattice parameters of each system were obtained by direct minimization of the total energy, with the atomic positions fully optimized until the interatomic forces were less than 10^{-3} eV/Å.

The same level was employed for the phonon calculations, for which we used the small displacement method as implemented in the Phon code [46]. The force constant matrix was computed using central differences within atomic displacements of 0.02 Å in 9×9 supercells.

Band structures have been calculated with G_0W_0 [47,48], considering SOC for all arsenic systems.

Relative stabilities have been calculated from single-point energies of optimized structures on the grounds of PBE-MBD and PBE0-MBD, which give different stacking orders and required calculations beyond DFT (see Table S1). We employed the RPA with the renormalized single excitation correction (RSE) [49] based on Kohn-Sham orbitals from the PBE and PBE0 level as implemented in FHI-AIMS [50] on tight tier 1 numeric atom-centered orbitals with added auxiliary diffuse basis functions on $12 \times 12 \times 1$ k grids to determine the most stable form. The RPA stacking orders are independent on the choice of the underlying density-functional (for comparison, see the Supplemental Material [30]), herein we discuss only the RPA + RSE@PBE0 variant. Relative energies ΔE (in meV per atom) are given with respect to the most stable stacking configuration, and interlayer binding energies E_{ib} are defined with respect to the monolayers.

This work was funded in Mexico by Cinvestav (Grant No. SEP-Cinvestav-2018-57). The CGSTIC (Xiuhcoatl) is acknowledged for allocation of computational resources. J. A. thanks Conacyt for support through her Ph.D. fellowship. We thank the Center for Information Services and High Performance Computing (ZIH) at TU Dresden for generous allocation of computer time. We thank BMBF (NobleNEMS) for financial support. We thank Andras Kis (EPFL) for fruitful discussions on 2D heterostructure manufacturing techniques.

*thomas.heine@tu-dresden.de
†gmerino@cinvestav.mx

[1] K. S. Novoselov, A. K. Geim, S. V. Morozov, D. Jiang, Y. Zhang, S. V. Dubonos, I. V. Grigorieva, and A. A. Firsov, Science **306**, 666 (2004).
[2] L. Britnell, R. V. Gorbachev, R. Jalil, B. D. Belle, F. Schedin, M. I. Katsnelson, L. Eaves, S. V. Morozov, A. S. Mayorov, N. M. Peres *et al.*, Nano Lett. **12**, 1707 (2012).
[3] P. Miró, M. Audiffred, and T. Heine, Chem. Soc. Rev. **43**, 6537 (2014).
[4] S.-J. An, Y. H. Kim, C. Lee, D. Y. Park, and M. S. Jeong, Sci. Rep. **8**, 1 (2018).
[5] S. Haastrup, M. Strange, M. Pandey, T. Deilmann, P. S. Schmidt, N. F. Hinsche, M. N. Gjerding, D. Torelli, P. M. Larsen, A. C. Riis-Jensen *et al.*, 2D Mater. **5**, 042002 (2018).
[6] H. Liu, A. T. Neal, Z. Zhu, Z. Luo, X. Xu, D. Tománek, and P. D. Ye, ACS Nano **8**, 4033 (2014).
[7] L. Li, Y. Yu, G. J. Ye, Q. Ge, X. Ou, H. Wu, D. Feng, X. H. Chen, and Y. Zhang, Nat. Nanotechnol. **9**, 372 (2014).
[8] Z. Zhu and D. Tománek, Phys. Rev. Lett. **112**, 176802 (2014).
[9] J. L. Zhang, S. Zhao, C. Han, Z. Wang, S. Zhong, S. Sun, R. Guo, X. Zhou, C. D. Gu, K. D. Yuan *et al.*, Nano Lett. **16**, 4903 (2016).
[10] C. Kamal and M. Ezawa, Phys. Rev. B **91**, 085423 (2015).
[11] L. Kou, Y. Ma, X. Tan, T. Frauenheim, A. Du, and S. Smith, J. Phys. Chem. C **119**, 6918 (2015).
[12] S. M. Beladi-Mousavi, A. M. Pourrahimi, Z. Sofer, and M. Pumera, Adv. Funct. Mater. **29**, 1807004 (2019).
[13] J. Xiao, M. Long, X. Zhang, J. Ouyang, H. Xu, and Y. Gao, Sci. Rep. **5**, 9961 (2015).
[14] S. Zhang, Z. Yan, Y. Li, Z. Chen, and H. Zeng, Angew. Chem., Int. Ed. Engl. **127**, 3155 (2015).
[15] H. Zhang, Y. Ma, and Z. Chen, Nanoscale **7**, 19152 (2015).
[16] Y.-p. Wang, C.-w. Zhang, W.-x. Ji, R.-w. Zhang, P. Li, P.-j. Wang, M.-j. Ren, X.-l. Chen, and M. Yuan, J. Phys. D **49**, 055305 (2016).
[17] Y. Cao, V. Fatemi, S. Fang, K. Watanabe, T. Taniguchi, E. Kaxiras, and P. Jarillo-Herrero, Nature (London) **556**, 43 (2018).

[18] Y. Cao, V. Fatemi, A. Demir, S. Fang, S. L. Tomarken, J. Y. Luo, J. D. Sanchez-Yamagishi, K. Watanabe, T. Taniguchi, E. Kaxiras *et al.*, Nature (London) **556**, 80 (2018).
[19] A. Kuc and T. Heine, Chem. Soc. Rev. **44**, 2603 (2015).
[20] R. Kempt, A. Kuc, and T. Heine, Angew. Chem. Int. Ed. **8**, 9242 (2020).
[21] K. Novoselov, A. Mishchenko, A. Carvalho, and A. H. Castro Neto, Science **353**, aac9439 (2016).
[22] M. I. Aroyo, A. Kirov, C. Capillas, J. Perez-Mato, and H. Wondratschek, Acta Crystallogr. Sect. A **62**, 115 (2006).
[23] J. E. Padilha and R. B. Pontes, J. Phys. Chem. C **119**, 3818 (2015).
[24] R. B. Pontes, R. H. Miwa, A. J. R. da Silva, A. Fazzio, and J. E. Padilha, Phys. Rev. B **97**, 235419 (2018).
[25] J. Ahn, I. Hong, Y. Kwon, R. C. Clay, L. Shulenburger, H. Shin, and A. Benali, Phys. Rev. B **98**, 085429 (2018).
[26] H. Cao, Z. Yu, and P. Lu, Superlattice Microstruct. **86**, 501 (2015).
[27] D. Kecik, E. Durgun, and S. Ciraci, Phys. Rev. B **94**, 205409 (2016).
[28] Y. Kadioglu, J. A. Santana, H. D. Özaydin, F. Ersan, O. Ü. Aktürk, E. Aktürk, and F. A. Reboredo, J. Chem. Phys. **148**, 214706 (2018).
[29] B.-J. Wang, X.-H. Li, R. Zhao, X.-L. Cai, W.-Y. Yu, W.-B. Li, Z.-S. Liu, L.-W. Zhang, and S.-H. Ke, J. Phys. Chem. A **6**, 8923 (2018).
[30] See the Supplemental Material at http://link.aps.org/supplemental/10.1103/PhysRevLett.125.196401 for details of the structure and energetics.
[31] L. Liang, J. Zhang, B. G. Sumpter, Q.-H. Tan, P.-H. Tan, and V. Meunier, ACS Nano **11**, 11777 (2017).
[32] F. Iyikanat, E. Torun, R. T. Senger, and H. Sahin, Phys. Rev. B **100**, 125423 (2019).
[33] Z. B. Aziza, V. Zólyomi, H. Henck, D. Pierucci, M. G. Silly, J. Avila, S. J. Magorrian, J. Chaste, C. Chen, M. Yoon *et al.*, Phys. Rev. B **98**, 115405 (2018).
[34] A. Kuc, T. Cusati, E. Dib, A. F. Oliveira, A. Fortunelli, G. Iannaccone, T. Heine, and G. Fiori, Adv. Electron. Mater. **3**, 1600399 (2017).
[35] P. Miró, M. Ghorbani-Asl, and T. Heine, Angew. Chem., Int. Ed. Engl. **53**, 3015 (2014).
[36] Y. Jing, Y. Ma, Y. Li, and T. Heine, Nano Lett. **17**, 1833 (2017).
[37] M. Ghorbani-Asl, A. Kuc, P. Miró, and T. Heine, Adv. Mater. **28**, 853 (2016).
[38] P. E. Blöchl, Phys. Rev. B **50**, 17953 (1994).
[39] G. Kresse and D. Joubert, Phys. Rev. B **59**, 1758 (1999).
[40] G. Kresse and J. Furthmüller, Comput. Mater. Sci. **6**, 15 (1996).
[41] G. Kresse and J. Furthmüller, Phys. Rev. B **54**, 11169 (1996).
[42] J. P. Perdew, K. Burke, and M. Ernzerhof, Phys. Rev. Lett. **77**, 3865 (1996).
[43] A. Tkatchenko, R. A. DiStasio, Jr., R. Car, and M. Scheffler, Phys. Rev. Lett. **108**, 236402 (2012).
[44] J. P. Perdew, M. Ernzerhof, and K. Burke, J. Chem. Phys. **105**, 9982 (1996).
[45] C. Adamo and V. Barone, Chem. Phys. Lett. **298**, 113 (1998).
[46] D. Alfè, Comput. Phys. Commun. **180**, 2622 (2009).
[47] L. Hedin, Phys. Rev. **139**, A796 (1965).
[48] M. Shishkin and G. Kresse, Phys. Rev. B **74**, 035101 (2006).
[49] X. Ren, P. Rinke, G. E. Scuseria, and M. Scheffler, Phys. Rev. B **88**, 035120 (2013).
[50] V. Blum, R. Gehrke, F. Hanke, P. Havu, V. Havu, X. Ren, K. Reuter, and M. Scheffler, Comput. Phys. Commun. **180**, 2175 (2009).